Site-specific valence-band photoemission study of α-Fe$_2$O$_3$

C.-Y. Kim and M. J. Bedzyk

*Department of Materials Science & Engineering and Institute for Environmental Catalysis, Northwestern University,
Evanston, Illinois 60208*

E. J. Nelson* and J. C. Woicik

National Institute of Standards and Technology, Gaithersburg, Maryland 20899

L. E. Berman

National Synchrotron Light Source, Brookhaven National Laboratory, Upton, New York 11973

We have measured the site-specific valence electronic structure of α-Fe$_2$O$_3$ by using a spatially modulated x-ray standing wave as the excitation source for photoemission. Contributions to the valence-band density of states from oxygen and iron ions are separated by this method. Both a bonding and nonbonding state originating from oxygen ions are obtained. The valence densities of states from iron agree well with predictions based on configuration-interaction cluster calculations by Fujimori *et al.* [Phys. Rev. B **34**, 1318 (1986)] which considered charge transfer from ligand to metal. The effects of strong hybridization between Fe and O valence states to x-ray emission and resonance photoemission are also evident.

There has been extensive study of the valence-band (VB) electronic structure of transition-metal (TM) oxides[1] since the discovery of the charge-transfer insulator nature of NiO.[2] Zaanen, Sawatzky, and Allen[3] developed a classification scheme using relative sizes of d-d Coulomb repulsion energies U (involved in $d_i^n d_j^n \rightarrow d_i^{n-1} d_j^{n+1}$ charge fluctuation) and charge-transfer energies $\Delta(d_i^n \rightarrow d_i^{n+1} L$, where L is ligand hole). According to this scheme, early TM (Ti, Cr, and Mn) oxides belong to Mott-Hubbard ($U < \Delta$) regime and late (Ni, Cu, and Zn) TM oxides belong to charge-transfer ($U > \Delta$) regime, and iron oxide is believed to be intermediate regime.

For α-Fe$_2$O$_3$, a general consensus has been established[4–7] about its charge-transfer insulator character since Fujimori's interpretation[4] and an observation of Fe $3d$ character of the lowest conduction band.[6] Most of the current information is based on Fe $3d$ derived states obtained from Fe $2p \rightarrow 3d$ resonance photoemission. The Fe $3d$ derived states in the VB region are assigned to the mixture of d^4, d^5L, and d^6L^2 (L^2 signifies two holes in the ligand) final states based on constant initial-state measurements and configuration-interaction (CI) cluster calculation.[4,5] However, the $3d$ derived states obtained by the resonance photoemission method contain significant contributions from hybridized O $2p$ states and there exists some disagreement about the oxygen $2p$ states.[4,5] Although the hybridization between the Fe $3d$ and O $2p$ states turned out to be essential to the charge-transfer nature, subsequent efforts to separate the contribution to the VB density of states due to individual elements have encountered difficulties caused by this very hybridization. The results from x-ray emission spectroscopy of O $K\alpha$ (Ref. 8) and Fe $L\alpha$ (Ref. 9) are also influenced by the strong hybridization effect. A hybridization between Fe $4sp$ and O (mostly $2p$ character) should also be considered for proper interpretation of the VB density of states. To our knowledge none of the approaches based on band structure

(i.e., reciprocal space) have been successful in a separation of the iron and oxygen contributions to the VB.

In this study, we used x-ray standing waves (XSW) for site-specific (i.e., direct space) valence-band photoemission from an α-Fe$_2$O$_3$ single crystal. Under the XSW condition the valence photocurrent can be approximated as the sum of partial density of states $\rho_{i,j}(E)$ from individual i atoms and j angular momentum components weighted by spatially varying electric-field intensities and by energy- and angular-momentum-dependent cross sections $\sigma_{i,j}(E,\hbar\omega)$ of each of state,[10] $I(E,\hbar\omega) \propto \Sigma_{i,j}\rho_{i,j}(E)\sigma_{i,j}(E,\hbar\omega)[1+R+2\sqrt{R}\cos(v-\mathbf{h}\cdot\mathbf{r}_i)]$. By changing the angle or incident photon energy, the standing-wave field node (or antinode) can be controllably positioned relative to the Bragg plane.[11] By collecting high-resolution valence photoemission spectra with a selectively located standing-wave field, spatially resolved valence-band densities of states are obtained.

For sample preparation, an α-Fe$_2$O$_3$ (0001) single crystal was cleaned by repeative Ar$^+$ sputtering (500 eV) and oxygen annealing. The sample temperature was measured by a thermocouple attached to the molybdenum sample holding clip. Depending on oxygen annealing conditions, surface structures as determined by low-energy electron diffraction were pure biphase (O$_2$ pressure at 3×10^{-6} torr with sample temperature at 760 °C) or a mixture of biphase and ($\sqrt{3} \times \sqrt{3}$) R30° phase (O$_2$ pressure at 1×10^{-6} torr with sample temperature at 700 °C).[12] Measurements were performed at the National Synchrotron Light Source X24A beamline. The XSW was generated by Bragg diffraction from the ($10\bar{1}4$) planes (Fig. 1) at a back-reflection geometry with photon energy of 2300 eV. X-ray photoelectrons were collected with a hemispherical analyzer with an exit angle of about 34° from the sample surface and with an overall experimental resolution of 0.3 eV. The valence photoelectron spectra were surface insensitive due to their high kinetic energy (~2300

(10$\bar{1}$4) Bragg planes

[0001]

[1000]
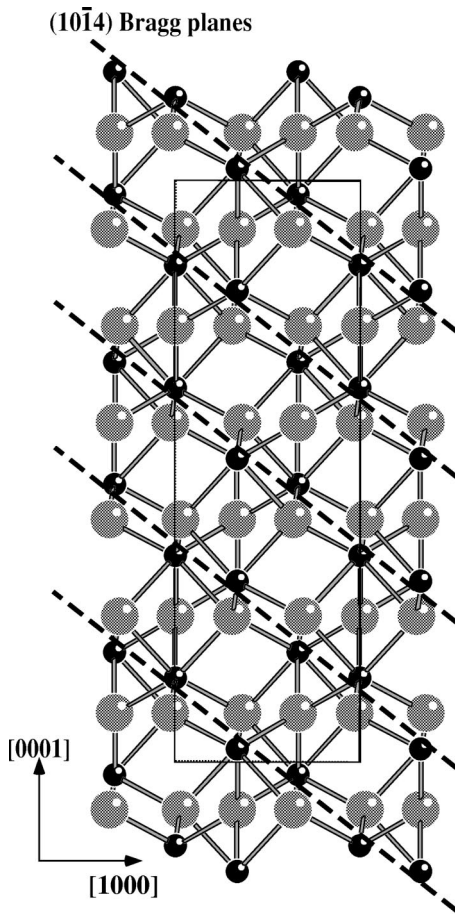
FIG. 1. Side view of α-Fe$_2$O$_3$(0001) crystal structure. Small filled dark circles and big circles correspond to iron and oxygen atoms, respectively. The (10$\bar{1}$4) Bragg planes are indicated by dashed lines and the unit cell is indicated by a solid rectangle.

FIG. 2. The experimental reflectivity, and photoelectron yields of O 1s and Fe 2$p_{3/2}$ from α-Fe$_2$O$_3$ obtained while scanning the photon energy through (10$\bar{1}$4) Bragg condition at a back-reflection geometry. The reflectivity signal is collected by the same photocurrent grid as the incident beam signal. The O 1s photoelectron yield was scaled to match the maximum of the Fe 2$p_{3/2}$ yield. The difference between the Fe and O yields was used to find the two energies (indicated with arrows) at which there is a maximum contrast between yields from Fe and O sites.

eV). There were no noticeable differences in spectra taken from the biphase surface and the mixed phase surface.

Figure 2 shows photoelectron yields from the Fe 2$p_{3/2}$ and O 1s core levels and the reflected x-ray intensity obtained by scanning the incident photon energy through the Bragg condition. The photoelectron yields were obtained by taking integrated intensities from selected electron energy regions. To get a maximum photoemission contrast between the Fe sites and O sites we choose two different incident photon energies corresponding to maximum (on-Fe) and minimum (off-Fe) to obtain a difference spectrum of normalized Fe and O photoelectron yield spectra. The maximum contrast was achieved by collecting spectra at photon energies $E_p - 0.16$ eV and $E_p + 0.23$ eV (E_p is the photon energy corresponding to reflectivity maximum). In Fig. 1 the lower energy places a XSW node on the (10$\bar{1}$4) diffraction plane and the higher energy places an antinode on this plane. These two energies are indicated with arrows in Fig. 2. To decompose the VB spectra into Fe and O components a normalization-subtraction procedure was used. First integrated intensities of Fe 3p and O 2s components were extracted from the raw spectra by fitting peaks with Voigt functions. As shown in Fig. 3, by subtracting the on-Fe spectrum

normalized with respect to the Fe 3p integrated intensity from the off-Fe spectrum normalized with respect to the Fe 3p integrated intensity a pure oxygen component was obtained. The Fe component was obtained in the same way by normalizing the raw spectra with the O 2s integrated intensities. The resulting decomposed spectra scaled to match the off-Bragg condition spectrum [Fig. 3(b)] shows a complete separation of the Fe 3p and O 2s core-level photoemission peaks. This serves as a validation check on the above described method. Figure 4 shows the detailed spectra in the VB region. Since the electric-field intensities at atomic core positions are proportional to core photoemission intensities, we can use the integrated intensities of Fe 3p and O 2s to reconstruct the VB spectrum taken at the off-Bragg condition ($E_p - 6.0$ eV). The Fe component at the off-Bragg condition can be obtained by multiplying the decomposed Fe component by the ratio of Fe 3p integrated intensities between off-Bragg and decomposed Fe spectrum. Similarly we obtained the off-Bragg O component, and the sum of the two components agrees well with the off-Bragg spectrum (not shown).

The Fe VB spectrum consists of four peaks located at binding energies of -2.7, -5.3, -8.0, and -12.4 eV. Our Fe VB spectrum agrees well with other experimental results derived by resonance photoemission measurements.[4,5] The agreement of our Fe spectrum with the CI cluster

(a)

(b)
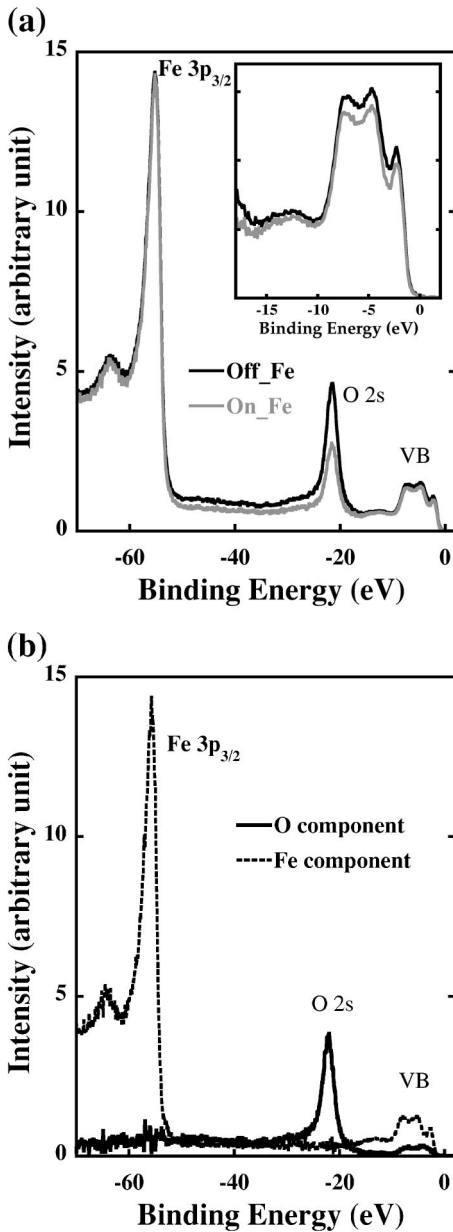
FIG. 3. (a) The site-specific photoemission spectra from Fe (on-Fe) and O sites (off-Fe) normalized with respect to the Fe $3p$ integrated intensities. The inset shows the VB region. (b) The decomposed spectra scaled to match the off-Bragg spectrum show a complete separation of photoelectrons from Fe and O ions.

calculation[4] (shown in the bottom of Fig. 4) is remarkable in relative intensities as well as in peak positions especially in the main band region (-2 to -10 eV). The peak intensity ratio of satellite (-12 to -18 eV) to main peak region in our measurement does not match with the calculation. Also there are noticeable differences in the peak intensity ratio of satellite to main peaks in our measurement taken with 2300 eV photons and in resonance photoemission taken at a photon energy around 60 eV.[4,5] This discrepancy can be understood by considering the different energy dependences of the photoionization cross sections $\sigma_{i,j}(E,h\omega)$ of the main and satellite peaks and agrees with the assignment of the main
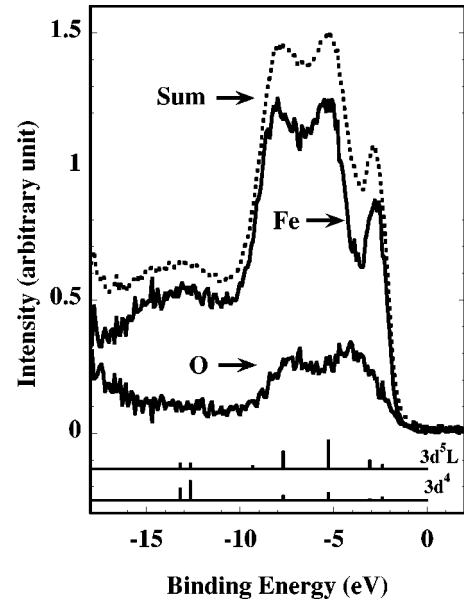
FIG. 4. The site-specific valence-band photoemission spectra from Fe and O sites along with their sum. The vertical lines at the bottom show the positions and relative intensities of the $3d^5L$ and $3d^4$ final states predicted in Ref. 4.

peaks to d^5L, d^6L^2 and of the satellite to the d^4 final states in the CI calculation. The VB spectrum that originated from oxygen ions consists of two peaks with binding energies at -4.0 and -7.2 eV. A similar O $2p$ X-ray photoemission spectrum was found for Al_2O_3.[13] The shallow one located at the position of minimum density of states from Fe site can be assigned to a nonbonding $2p$ component. The deeper one that matches well with Fe $4p$ states reported based on Fe $K\beta_{2,5}$ emission[9] can be assigned to a bonding state with Fe $4p$ (and possibly $4s$). The photoemission spectrum with two components is quite different from the traditional assignments of photoemission spectra taken at low photon energies (<40 eV) to oxygen spectra.[5,14] This assignment was based on a steep increase of the oxygen photoionization cross section and gradual decrease of cation cross section at a low-excitation photon energy. The discrepancy can be explained by the hybridization between O $2p$ and cation valence states that gives a significant contribution from the cation even at a low photon energy.[4]

Since the difference spectrum in resonance photoemission is made of unhybridized Fe $3d$ states and hybridized states with O $2p$, the differences between VB photoemission from the Fe site and the spectrum derived from resonance photoemission correspond to contributions from the hybridized O $2p$ component (in resonance photoemission) and Fe $4sp$ components. Indeed, the Fe $3d$ derived spectrum deduced from resonance photoemission[5] has a significant amount of an extra component around the O $2p$ bonding state at 8 eV in addition to the spectrum from the Fe sites. It appears that the oxygen bonding state at 8 eV is also involved in bonding with $3d^5L$ states.

There has been an attempt to obtain the oxygen contribution to the VB by using O $K\alpha$ emission.[8] The emission spectrum consists of three peaks with the main peak at 5 eV and

shoulders at 3 and 8 eV from the valence-band top. As pointed out in the above paper, the final state of O $K\alpha$ emission is the d^5L state and the O $K\alpha$ emission spectrum was well explained by the Fe $3d$ derived states. Again the main peak at 5 eV is dominated by hybridization with Fe states. It is worth noting that the O $K\alpha$ spectrum is quite similar to the VB photoemission taken at a low photon energy. Although we speculate that the shoulders may originate from the O $2p$ states located at -4.0 and -7.2 eV, it is not certain at this stage.

In summary we used site-specific valence-band photoemission to separate the contribution from individual Fe and O atoms to the valence-band density of states of α-Fe$_2$O$_3$. Due to the spatial resolving power of XSW, we were able to experimentally obtain the oxygen valence states of α-Fe$_2$O$_3$. The O $2p$ states are composed of two states of bonding and nonbonding characters similar to other metal oxides. The Fe component in the VB was obtained at the same time and it agrees well with the Fe $3d$ derived states of a previous Cl cluster calculation that takes into account the mixture of the d^4, d^5L, and d^6L^2 final states of iron ion.

---

*Present address: Glenn T. Seaborg Institute, Lawrence Livermore National Laboratory, P.O. Box 808 MS L-231, Livermore, CA 94551.

[1] P. A. Cox, *The Transition Metal Oxides* (Oxford University Press, Oxford, 1992).

[2] G. A. Sawatzky and J. W. Allen, Phys. Rev. Lett. **53**, 2339 (1984).

[3] J. Zaanen, G. A. Sawatzky, and J. W. Allen, Phys. Rev. Lett. **55**, 418 (1985).

[4] A. Fujimori, M. Saeki, N. Kimuzuka, M. Taniguchi, and S. Suga, Phys. Rev. B **34**, 7318 (1986).

[5] R. J. Lad and V. E. Henrich, Phys. Rev. B **39**, 13 478 (1989).

[6] F. Ciccacci, L. Braicovich, E. Puppin, and E. Vescovo, Phys. Rev. B **44**, 10 444 (1991).

[7] M. Catti, G. Valerio, and R. Dovesi, Phys. Rev. B **51**, 7441 (1995).

[8] Y. Ma, P. D. Johnson, N. Wassdashl, J. Guo, P. Skytt, J. Nordgren, S. D. Keven, J.-E. Rubensson, T. Böske, and W. Eberhardt, Phys. Rev. B **48**, 2109 (1993).

[9] G. Dräger, W. Czolbe, and J. A. Leiro, Phys. Rev. B **45**, 8283 (1992).

[10] J. C. Woicik, E. J. Nelson, D. Heskett, J. Warner, L. E. Berman, B. A. Karlin, L. A. Vartanyants, M. Z. Hasan, T. Kendelewicz, Z. X. Shen, and P. Pianetta, Phys. Rev. B **64**, 125115 (2001).

[11] B. W. Batterman and H. Cole, Rev. Mod. Phys. **36**, 681 (1964).

[12] A. Barbieri, W. Weiss, M. A. Van Hove, and G. A. Somorjai, Surf. Sci. **302**, 259 (1994).

[13] A. Balzarotti and A. Bianconi, Phys. Status Solidi B **76**, 689 (1976).

[14] J. J. Yeh and I. Lindau, At. Data Nucl. Data Tables **32**, 1 (1985).